Phase-field-based lattice Boltzmann method for containerless freezing

Jiangxu Huang,[1] Lei Wang,[2] Zhenhua Chai,[1,3,4,*] and Baochang Shi[1,3,4]

[1]*School of Mathematics and Statistics, Huazhong University of Science and Technology, Wuhan 430074, China*

[2]*School of Mathematics and Physics, China University of Geosciences, Wuhan 430074, China*

[3]*Institute of Interdisciplinary Research for Mathematics and Applied Science, Huazhong University of Science and Technology, Wuhan 430074, China*

[4]*Hubei Key Laboratory of Engineering Modeling and Scientific Computing, Huazhong University of Science and Technology, Wuhan 430074, China*

(Received 6 May 2024; accepted 8 August 2024; published 6 September 2024)

In this paper we first propose a phase-field model for the containerless freezing problems, in which the volume expansion or shrinkage of the liquid caused by the density change during the phase change process is considered by adding a mass source term to the continuum equation. Then a phase-field-based lattice Boltzmann (LB) method is further developed to simulate solid-liquid phase change phenomena in multiphase systems. We test the developed LB method by the problem of conduction-induced freezing in a semi-infinite space, the three-phase Stefan problem, and the droplet solidification on a cold surface, and the numerical results are in agreement with the analytical and experimental solutions. In addition, the LB method is also used to study the rising bubbles with solidification. The results of the present method not only accurately capture the effect of bubbles on the solidification process, but also are in agreement with the previous work. Finally, a parametric study is carried out to examine the influences of some physical parameters on the sessile droplet solidification, and it is found that the time of droplet solidification increases with the increase of droplet volume and contact angle.

DOI: 10.1103/PhysRevE.110.035301

I. INTRODUCTION

Solidification or freezing, as a common solid-liquid phase change phenomenon, is of significant importance in nature and industrial applications [1,2], such as refrigeration [3], aerospace [4], additive manufacturing [5], and food processing [6]. In the past decades, many theoretical and experimental studies have been conducted to investigate the fluid flows and heat transfer during solidification process. However, the solidification often occurs in an ambient fluid, where the phase change process and interaction with the surrounding fluid need to be considered [7,8]. This process involves the gas, liquid, and solid phases, and the dynamic evolution of the phase interfaces, as well as the coupling of flow and heat transfer, brings some significant challenges to the study of solidification in multiphase systems.

A single droplet freezing on the cold substrate has been widely considered as a fundamental problem to explore the underlying freezing mechanism. Up to now some experimental work has been performed to investigate the droplet freezing process on the cold substrate [9–17]. In 1996 Anderson *et al.* [9] first discovered that the freezing droplet forms a tip and reported that only a dynamic growth angle could predict the inflection point of a freezing droplet. Subsequently, Schultz *et al.* [10] found that the droplet tip results from a combination of expansion and phase boundary curvature during freezing. Then Ajaev and Davis [11] extended this work to the pendant droplets. Recently, Hu *et al.* [12] experimentally studied the the droplet freezing on the cold substrate based on the molecular labeling thermometry technique. The results show that the volume of water droplet expands during freezing and the expansion mainly in the upward direction rather than the radial direction. Chaudhary *et al.* [13] experimentally investigated the freezing of water droplet on a cooled surface. They used an infrared camera and thermocouple to measure the temperature evolution of the frozen droplet and observed four distinct processes: liquid cooling, recalescence, freezing, and solid cooling. Enríquez and Marin [14,15] found that the liquid-solid interface of the water droplet expands during the freezing process, causing the droplet to form a pointed tip at the top, which is a consequence of a self-similar geometric mechanism, independent of the solidification. Based on the work of Marin *et al.* [15], Schremb *et al.* [16] proposed a new experimental method to study the solidification of a supercooled droplet using the Hele-Shaw cell, and this method allows observation of the process in a quasi-two-dimensional manner, without optical distortions arising from the free surface of the droplet. The experimental results show that the a small mutual influence of the dendrites is observed only when the freezing process is dominated by heat diffusion and supercooling is high. More recently, Zeng *et al.* [17] investigated the influence of gravity on the freezing of pendent and sessile droplets through an experimental method. They demonstrated that the gravity significantly affects the droplet freezing process by shaping the initial droplet, resulting in the flattening or elongation of pendent and sessile droplet, respectively.

*Contact author: hustczh@hust.edu.cn

Although experimental methods can be used to obtain external and internal information of a frozen droplet through direct physical observation and measurement, due to the limitations of measurement techniques, it is difficult to obtain detailed information on the internal icing front, temperature field, and velocity and pressure distributions inside the droplet. In particular, although the intrusive measurement method can obtain information about the interior of the droplet, the measurement probe may affect the icing process. Therefore, in order to overcome the limitations of experimental methods, it is necessary to develop accurate theoretical models or numerical methods to derive more detailed information about the interior of frozen droplet. Through considering the effects of supercooling and gravity, Zhang *et al.* [18] developed a theoretical model to investigate the freezing behavior of a water droplet and compared it with experiments. It was found that the freezing rate and time, as well as the droplet profile calculated by the model, are in good agreement with the experimental results. Based on a one-dimensional approximation, Tembely *et al.* [19] proposed a theoretical and numerical method to simulate droplet freezing on cold hydrophilic surfaces, and the model accurately predict the freezing time, droplet volume expansion, and tip singularity during freezing. Zhu *et al.* [20] conducted the experimental and theoretical studies on the freezing characteristics of water droplet deposited on the cold hydrophilic and hydrophobic aluminum surfaces. The results show that the freezing shape of sessile droplet depends on the surface temperature and wettability, and a power-law relationship between the freezing time of deposited droplet and the surface temperature was obtained. Although the theoretical models can be used to predict the freezing time, volume expansion, and tip singularity that are consistent with experiment, they often rely on simplifying assumptions. For example, in the models of Zhang *et al.* [18] and Zhu *et al.* [20], the freezing front is always assumed to be flat, which is clearly unreasonable; while in the theoretical model of Tembely *et al.* [19], the lubrication approximation is usually applicable to the hydrophilic configurations. In addition, the dynamic evolution and strong nonlinear properties of phase interfaces also bring some challenges to the theoretical analysis.

To overcome the limitations of the experimental and theoretical approaches, some numerical methods have been developed to study the solidification processes in multiphase systems [21–29]. Vu *et al.* [21] and Shetabivash *et al.* [22] simulated the solidification of sessile droplets on a cold plate by the front-tracking method and multiple level-set approaches. In their works the droplet volume change due to density variation during solidification is taken into account, and the angle at the trijunction point can also be imposed. Lyu *et al.* [23] developed a novel hybrid volume-of-fluid and immersed-boundary (VOF-IB) method to simulate freezing droplet considering the volume expansion during freezing, and tested the accuracy of the method through a comparison with some available experimental and theoretical results. The numerical results in their work also show that the lower the density ratio, the longer the freezing time, and the more likely the formation of singular tips at the end of the freezing stage. Different from these traditional numerical methods, the kinetic theory-based LB method has been widely used to study phase change problems due to its simple algorithmic structure, high parallelism, and ability to handle complex physics and boundary conditions [24–30]. For example, Sun *et al.* [24] and Zhang *et al.* [25] investigated droplet solidification on the cold surface using the multiphase-field pseudopotential LB method, the main difference between these two works being that the volume change of the droplet during the freezing process is not taken into account in the work of Sun *et al.* [24]. Xiong *et al.* [26,27] also employed the pseudopotential LB method to study the impact dynamics and solidification behavior of droplet on cold smooth and rough substrates. However, it is known that the pseudopotential LB method usually suffers from the numerical instability for the multiphase problems with large-density ratios [30]. To resolve this problem, the phase-field base LB method is adopted to study the freezing process of the droplet. For example, Zhang *et al.* [28] proposed a phase-field based LB method to study the ice evolution during methane hydrate dissociation, while the volume change of a droplet has not been considered. To overcome this drawback, Mohammadipour *et al.* [29] developed another phase-field based LB method to investigate the solidification behavior of droplets in multicomponent systems, and considered the volume change of droplets during the solidification process by adding a mass source term to the Cahn-Hilliard (CH) equation. However, it should be noted that in the framework of LB method, the fourth-order C-H equation cannot be recovered correctly [31].

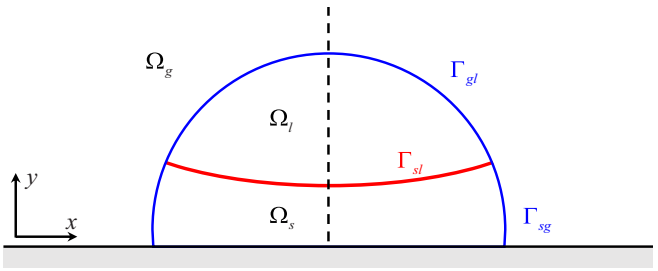

FIG. 1. Schematic of a freezing droplet on the cold substrate.

In this work, we will propose a phase-field based LB method to study containerless freezing problems, and simultaneously, the volume change during solidification can be taken into account. Different from the previous work [29], here we considered a new second-order Allen-Cahn (A-C) equation where the volume change during solidification is included through adding a mass source term based on mass conservation. Additionally, the present LB method has more advantages in the study of multiphase flows with larger density ratios since it can capture the topological changes of the interfaces more accurately. The remainder of this paper is organized as follows. In Sec. II a mathematical model for the containerless freezing problems is proposed, followed by the developed phase-field LB method in Sec. III. Numerical results and discussion are presented in Sec. IV, and finally, a brief summary is given in Sec. V.

II. MATHEMATICAL MODEL

We now take the freezing process of a droplet on the cold substrate as an example, as shown in Fig. 1, and assume that the solid phase forms only within the liquid phase; the liquid

and gas phase fluids are immiscible. The freezing process occurring in an ambient gas environment is a gas-liquid-solid ternary phase system, and the solid-liquid (Γ_{sl}), solid-gas (Γ_{sg}), and gas-liquid (Γ_{gl}) interfaces must be updated simultaneously. To simplify the following analysis, the phase interfaces can be divided into the one with phase change (Γ_{sl}) and those without phase change (Γ_{sg}, Γ_{gl}). The basic idea of the present work is to use the phase-field method to track interfaces without phase change, and update the interface with phase change using the enthalpy method. To this end, the phase-field order parameter, ϕ, is introduced to distinguish whether the medium is solid-liquid mixture or gas phase. Here $\phi = 1$ represents the solid-liquid mixtures, and $\phi = 0$ denotes the surrounding gas phase. On the other hand, the solid fraction used in the enthalpy method, f_s, is adopted to label the interface between the solid and liquid phases in solid-liquid mixtures, where $f_s = 1$ stands for the solid phase and $f_s = 0$ denotes the liquid phase. With the help of the order parameter ϕ and solid fraction f_s, the liquid, solid, and gas phases can be represented by ($\phi = 1$ and $f_s = 0$), ($\phi = 1$ and $f_s = 1$) and ($\phi = 0$ and $f_s = 0$). In this case, the physical properties of system can be characterized by a linear function of the order parameter and solid fraction:

$$\zeta = f_s\zeta_s + (1 - f_s)\phi\zeta_l + (1 - f_s)(1 - \phi)\zeta_g, \tag{1}$$

where the parameter ζ denotes the density, viscosity, thermal conductivity, and heat capacity, and the subscripts g, l, and s, represent the gas, liquid, and solid phases, respectively.

In the following, we will propose a mathematical model for containerless freezing processes, which includes the phase-field equation, enthalpy based energy equation, and Navier-Stokes equations.

A. Phase-field method for capturing interfaces without phase change

The Allen-Cahn equation has been widely used to model moving interfaces among different phases [28,32], and for the interfacial dynamics without phase change (Γ_{sg}, Γ_{gl}), it can be written as

$$\frac{\partial\phi}{\partial t} + \nabla\cdot(\phi\mathbf{u}) = \nabla\cdot[M(\nabla\phi - \lambda\mathbf{n})] + \phi\nabla\cdot\mathbf{u}, \tag{2}$$

where ϕ is the order parameter, $\mathbf{u}$ is the velocity, M is a positive constant called mobility, $\mathbf{n} = \nabla\phi/|\nabla\phi|$ is the unit vector normal to the interface, and λ is a function of ϕ and is defined as

$$\lambda = \frac{4\phi(1 - \phi)}{W}, \tag{3}$$

where W is the interface thickness. It should be noted that for incompressible fluid flows, the last term on the right-hand side of Eq. (2) can be neglected, while for the freezing process including the volume change, it must be considered (see the following discussion).

B. The Navier-Stokes equations for fluid flows

Apart from the interface-capturing equation mentioned above, we now introduce the governing equations for fluid flows. We assumed the fluid to be immiscible and Newtonian, and the fluid flows can be described by the following Navier-Stokes (N-S) equations [32,33]:

$$\nabla\cdot\mathbf{u} = 0, \tag{4a}$$

$$\frac{\partial\rho\mathbf{u}}{\partial t} + \nabla\cdot(\rho\mathbf{u}\mathbf{u}) = -\nabla p + \nabla\cdot\{\mu[\nabla\mathbf{u} + (\nabla\mathbf{u})^{\mathrm{T}}]\} + \mathbf{F}_s + \mathbf{G}, \tag{4b}$$

where ρ is the density, p is the pressure, μ is the dynamic viscosity, $\mathbf{G}$ is the body force, and $\mathbf{F}_s$ is the surface tension force,

$$\mathbf{F}_s = \mu_\phi\nabla\phi, \tag{5}$$

where μ_ϕ is the chemical potential and is defined by

$$\mu_\phi = 4\beta(\phi - \phi_l)(\phi - \phi_g)\left(\phi - \frac{\phi_l + \phi_g}{2}\right) - \kappa\nabla^2\phi. \tag{6}$$

The physical parameters β and κ are related to the interface thickness W and the surface tension σ,

$$k = \frac{3}{2}\sigma W, \quad \beta = \frac{12\sigma}{W}. \tag{7}$$

During the freezing process, the droplet volume may expand or shrink because of the density difference between solid and liquid phases [12,15]. In order to include the volume change into the above N-S equations, some modifications have been made to the continuity equation by neglecting the gas phase to account for the density change during the solidification of liquid-solid mixtures [22,23,34]. Here we make a similar assumption adopted in the VOF and level-set frameworks through considering mixture of the three phases of liquid, solid, and gas. Actually, in an arbitrary control volume with the constant mass that consists of both solid and liquid phases, the conservation of mass can be expressed as

$$\frac{D}{Dt}(M) = \frac{D}{Dt}(M_l + M_s) = 0, \tag{8}$$

where the solid and liquid masses are defined as

$$M_s = \int_{V_s(t)}\rho_s\,dV_s = \int_{V(t)}\rho_s f_s\,dV, \tag{9a}$$

$$M_l = \int_{V_l(t)}\rho_l\,dV_l = \int_{V(t)}\rho_l(1 - f_s)\,dV, \tag{9b}$$

substituting Eqs. (9a) and (9b) in (8), we can obtain

$$\frac{D}{Dt}\left\{\int_{V(t)}[\rho_s f_s + \rho_l(1 - f_s)]dV\right\} = 0. \tag{10}$$

Using Reynolds' transport theorem and assuming zero velocity in the solid phase, we have

$$\int_{V(t)}\left\{\frac{\partial}{\partial t}(\rho_s f_s) + \nabla\cdot[(1 - f_s)\rho_l\mathbf{u}_l] - \frac{\partial}{\partial t}(\rho_l f_s)\right\}dV = 0, \tag{11}$$

where $\mathbf{u}_l$ is the liquid velocity. To ensure the integral over any integration region $V_{(t)}$ to be zero, one can obtain

$$\nabla\cdot[(1 - f_s)\mathbf{u}_l] = \left(1 - \frac{\rho_s}{\rho_l}\right)\frac{\partial f_s}{\partial t}. \tag{12}$$

Using the fact $\mathbf{u} = \mathbf{u}_l(1 - f_s) + \mathbf{u}_s f_s$, we can rewrite the above equation as

$$\nabla\cdot\mathbf{u} = \dot{m}, \tag{13}$$

where the source term $\dot{m} = (1 - \frac{\rho_s}{\rho_l})\frac{\partial f_s}{\partial t}$ on the right-hand side of Eq. (13) describes the expansion or shrinkage of the volume during the freezing process, and it is influenced by the ratio of solid density to liquid density.

In addition, how to treat the fluid-solid boundary is also a crucial issue. To overcome the difficulty in directly treating the solid-fluid interface, Noble and Torczynski [35] proposed an immersed moving boundary approach, which has also been widely used to deal with solid-liquid phase change problems [36,37]. To characterize the interaction between fluid and solid more accurately, a diffuse-interface method is further developed through adding a modified force term to the momentum equation [38]. In this method, the momentum equation can be written as

$$\frac{\partial \rho \mathbf{u}}{\partial t} + \nabla \cdot (\rho \mathbf{u}\mathbf{u}) = -\nabla p + \nabla \cdot \{\mu[\nabla \mathbf{u} + (\nabla \mathbf{u})^{\mathrm{T}}]\} + \mathbf{F}_s + \mathbf{G} + \rho \mathbf{f}, \tag{14}$$

where $\mathbf{f}$ is the force generated by fluid-solid interaction to be discussed below.

C. Enthalpy method for moving interface

The temperature equation used to describe the freezing front (Γ_{sl}) can be derived from the energy conservation [39,40],

$$\frac{\partial(\rho h)}{\partial t} + \nabla \cdot (\rho h \boldsymbol{u}) = \nabla \cdot (\lambda \nabla T) + \rho h \nabla \cdot \mathbf{u} + \dot{q}, \tag{15}$$

where T, C_p, and λ are temperature, specific heat at constant pressure, and thermal conductivity. $h = C_p T$ is the sensible enthalpy. $\dot{q}$ is the heat source term caused by the absorption or release of latent heat and can be given by [40]

$$\dot{q} = -\left[\frac{\partial(\rho \Delta H)}{\partial t} + \nabla \cdot (\rho \boldsymbol{u} \Delta H)\right], \tag{16}$$

where ΔH is the latent enthalpy undergoing phase change. For the pure material freezing, the second term $\nabla \cdot (\rho \boldsymbol{u} \Delta H)$ can be neglected due to the uniform latent heat of the liquid, and thus $\dot{q}$ can be simplified as [40]

$$\dot{q} = -\frac{\partial(\rho \Delta H)}{\partial t} = -\frac{\partial(\rho L f_l)}{\partial t}, \tag{17}$$

where L is the latent heat, and f_l is the liquid fraction, given by $f_l = \Delta H / L$. Substituting Eq. (15) into Eq. (17), one can obtain [39,40]

$$\frac{\partial(\rho H)}{\partial t} + \nabla \cdot (\rho C_p T \mathbf{u}) = \nabla \cdot (\lambda \nabla T) + \rho C_p T \nabla \cdot \mathbf{u}, \tag{18}$$

where H is the total enthalpy, which can be divided into the sensible and latent enthalpy components as

$$H = h + \Delta H = C_p T + L f_l. \tag{19}$$

Based on above definition of total enthalpy, the liquid fraction and temperature can be calculated as follows [41]:

$$f_l = \begin{cases} 0, & H \leqslant H_s \\ \frac{H - H_s}{H_l - H_s}, & H_s \leqslant H \leqslant H_l \\ 1, & H \geqslant H_l \end{cases}, \tag{20a}$$

$$T = \begin{cases} H/C_p & H < H_s \\ T_s + \frac{H - H_s}{H_l - H_s}(T_l - T_s) & H_s \leqslant H \leqslant H_l \\ T_l + (H - H_l)/C_p & H > H_l \end{cases}, \tag{20b}$$

where T_s and T_l are the solidus and liquidus temperatures, respectively, and $H_s = C_{p,s} T_s$ and $H_s = C_{p,l} T_l + L$ are the total enthalpy at the solidus and liquidus temperatures. Through solving the enthalpy-based energy equation (18), one can not only obtain the temperature field, but also simultaneously determine the liquid fraction, thereby achieving implicit tracking of the solid-liquid phase interface. In summary, the present mathematical model, including Eqs. (2), (13), (14), and (18), is used to describe the droplet freezing process, and the volume change is also considered.

III. LB METHOD FOR CONTAINERLESS FREEZING

In this section, we will develop a new LB method where three different LB models are adopted for phase field, temperature field, and flow field.

A. LB model for the phase field

The evolution equation of LB model with the BGK collision operator for the Allen-Cahn equation can be written as [32]

$$g_i(\mathbf{x} + \mathbf{c}_i \Delta t, t + \Delta t) - g_i(\mathbf{x}, t) = -\frac{1}{\tau_g}\left[g_i(\mathbf{x}, t) - g_i^{\mathrm{eq}}(\mathbf{x}, t)\right] + \left(1 - \frac{1}{2\tau_g}\right)\Delta t G_i(\mathbf{x}, t), \tag{21}$$

where $g_i(\mathbf{x}, t)$ is the order parameter distribution function at position $\mathbf{x}$ and time t, and $\mathbf{c}_i$ is the discrete velocity. For the D2Q9 model considered here, the weight coefficient ω_i and discrete velocity $\mathbf{c}_i$ are defined as

$$\omega_i = \begin{cases} 4/9 & i = 0, \\ 1/9 & i = 1 - 4, , \\ 1/36 & i = 5 - 8, \end{cases} \tag{22}$$

$$\mathbf{c}_i = \begin{cases} (0, 0), & i = 0, \\ (\cos[(i-1)\pi/2], \sin[(i-1)\pi/2])c, & i = 1 - 4, \\ (\cos[(2i-9)\pi/4], \sin[(2i-9)\pi/4])\sqrt{2}c, & i = 5 - 8, \end{cases} \tag{23}$$

where $c = \Delta x/\Delta t$ is the lattice speed with Δx and Δt denoting the lattice spacing and time step, respectively (both of them are set to 1 in the present work). $g_i^{\rm eq}$ is the equilibrium distribution and is given by

$$g_i^{\rm eq} = \omega_i \phi \left(1 + \frac{\mathbf{c}_i \cdot \mathbf{u}}{c_s^2}\right), \tag{24}$$

where $c_s = c/\sqrt{3}$ is the sound speed. To recover the Allen-Cahn equation with the multiscale analysis, the source term G_i should be designed as

$$G_i = \frac{\omega_i \mathbf{c}_i \cdot \left[\partial_t(\phi \mathbf{u}) + c_s^2 \lambda \mathbf{n}\right]}{c_s^2} + \omega_i \phi \nabla \cdot \mathbf{u}. \tag{25}$$

In addition, the order parameter in the present LB model can be computed by

$$\phi = \sum_i g_i + \frac{\Delta t}{2} \phi \nabla \cdot \mathbf{u}. \tag{26}$$

Following the Chapman-Enskog analysis, the Allen-Cahn equation can be recovered correctly from the LB model (21) with the mobility $M = c_s^2(\tau_f - 0.5)\Delta t$.

B. LB model for the temperature field

For the temperature field, the enthalpy-based thermal LB model proposed by Huang *et al.* [40] is adopted, and the evolution equation of the total enthalpy distribution function $h_i(\mathbf{x}, t)$ reads

$$\begin{aligned} &h_i(\mathbf{x} + \mathbf{e}_i \Delta t, t + \Delta t) \\ &\quad = h_i(\mathbf{x}, t) - \frac{1}{\tau_h}\left[h_i(\mathbf{x}, t) - h_i^{\rm eq}(\mathbf{x}, t)\right] \\ &\qquad + \left(1 - \frac{1}{2\tau_h}\right)\Delta t \rho h \dot{m}, \end{aligned} \tag{27}$$

where $\tau_h = \lambda/\rho C_{p,\rm ref}\, c_s^2 \Delta t + 0.5$ is the relaxation time related to the thermal conductivity, and $h_i^{\rm eq}$ is the local equilibrium distribution function [40],

$$h_i^{\rm eq} = \begin{cases} H - C_{p,\,\rm ref}\, T + \omega_i C_p T\left(\frac{C_{p,\rm ref}}{C_p} - \frac{\mathbf{I}:\mathbf{uu}}{2c_s^2}\right), & i = 0, \\ \omega_i C_p T\left[\frac{C_{p,\,\rm ref}}{C_p} + \frac{\mathbf{e}_i \cdot \mathbf{u}}{c_s^2} + \frac{(\mathbf{e}_i\mathbf{e}_i - c_s^2\mathbf{I}):\mathbf{uu}}{2c_s^4}\right], & i \neq 0, \end{cases} \tag{28}$$

where $C_{p,\,\rm ref}$ is the harmonic mean of solid phase specific heat $C_{p,s}$ and liquid phase specific heat $C_{p,l}$. The total enthalpy is is calculated by

$$H = \sum_{i=0} h_i + \frac{1}{2}\Delta t \rho h \dot{m}. \tag{29}$$

C. LB model for the flow field

Differently from the original LB model for the flow field, we incorporate an extra mass source arising from density change during the freezing process, which results in some modifications to the evolution equation and the computation of macroscopic quantities. The evolution equation of the LB model for flow field is formulated as follows [42]:

$$\begin{aligned} &f_i(\mathbf{x} + \mathbf{c}_i \Delta t, t + \Delta t) - f_i(\mathbf{x}, t) \\ &\quad = -\frac{1}{\tau_f}\left[f_i(\mathbf{x}, t) - f_i^{\rm eq}(\mathbf{x}, t)\right] + \Delta t\left(1 - \frac{1}{2\tau_f}\right)F_i(\mathbf{x}, t), \end{aligned} \tag{30}$$

where $\tau_f = \nu/{c_s}^2 \Delta t + 0.5$ is the corresponding relaxation time for flow field, and $f_i^{\rm eq}$ is the local equilibrium distribution function,

$$f_i^{\rm eq} = \begin{cases} \frac{p}{c_s^2}(\omega_i - 1) + \rho s_i(\mathbf{u}), & \mathrm{i} = 0 \\ \frac{p}{c_s^2}\omega_i + \rho s_i(\mathbf{u}), & \mathrm{i} \neq 0 \end{cases} \tag{31}$$

with

$$s_i(\mathbf{u}) = \omega_i\left[\frac{\mathbf{c}_i \cdot \mathbf{u}}{c_s^2} + \frac{(\mathbf{c}_i \cdot \mathbf{u})^2}{2c_s^4} - \frac{\mathbf{u} \cdot \mathbf{u}}{2c_s^2}\right]. \tag{32}$$

The forcing term F_i is given by [42]

$$F_i = \omega_i\left[S + \frac{\mathbf{c}_i \cdot (\mathbf{F} + \rho \mathbf{f})}{c_s^2} + \frac{(\mathbf{u}\tilde{\mathbf{F}} + \tilde{\mathbf{F}}\mathbf{u}) : \left(\mathbf{c}_i\mathbf{c}_i - c_s^2\mathbf{I}\right)}{2c_s^4}\right], \tag{33}$$

where $S = \rho \dot{m} + \mathbf{u} \cdot \nabla \rho$, $\tilde{\mathbf{F}} = \mathbf{F} - \nabla p + c_s^2 \nabla \rho + c_s^2 \nabla \cdot S$, $\mathbf{F} = \mathbf{F}_{\rm s} + \mathbf{G}$ is the total force. The macroscopic velocity $\mathbf{u}$ and pressure p can be evaluated by

$$\rho \mathbf{u}^* = \sum \mathbf{c}_i f_i + \frac{\Delta t}{2}\mathbf{F}, \tag{34}$$

$$\mathbf{u} = \mathbf{u}^* + \frac{\Delta t}{2}\mathbf{f}, \tag{35}$$

$$p = \frac{c_s^2}{(1 - \omega_0)}\left[\sum_{i \neq 0} f_i + \frac{\Delta t}{2} S + \tau \Delta t F_0 + \rho s_0(\mathbf{u})\right], \tag{36}$$

where $\mathbf{u}^*$ is the velocity without considering the fluid-particle interaction, and $\mathbf{u}$ is the corrected velocity. The fluid-solid interaction force $\mathbf{f}$ can be discretized as $f_s(\mathbf{u}_s - \mathbf{u}^*)/\Delta t$ [38], where $\mathbf{u}_s$ is the solid-phase velocity. We would like to point out that this treatment has been successfully applied to deal with a variety of fluid-solid coupling problems, such as the particulate flows [38], dendrite growth [43], and two-phase flow in complex structures [44].

In numerical simulations, the derivative terms should be discretized with some suitable difference schemes. For simplicity, the temporal derivative in Eq. (25) is approximated by the first-order explicit Euler scheme [45],

$$\partial_t(\phi \mathbf{u})(\mathbf{x}, t) = [(\phi \mathbf{u})(\mathbf{x}, t) - (\phi \mathbf{u})(\mathbf{x}, t - \Delta t)]/\Delta t. \tag{37}$$

To calculate the gradient and Laplace operators appeared above, the second-order isotropic central schemes are applied [32,45]:

$$\nabla \zeta(\mathbf{x}, t) = \sum_{i \neq 0} \frac{\omega_i \mathbf{c}_i \zeta(\mathbf{x} + \mathbf{c}_i \Delta t, t)}{c_s^2 \Delta t}, \tag{38a}$$

$$\nabla^2 \zeta(\mathbf{x}, t) = \sum_{i \neq 0} \frac{2\omega_i[\zeta(\mathbf{x} + \mathbf{c}_i \Delta t, t) - \zeta(\mathbf{x}, t)]}{c_s^2 \Delta t^2}. \tag{38b}$$

D. Numerical implementation of the wetting boundary condition

In the presence of gas-liquid-solid interaction, the fluid interface dynamics would be greatly affected by the wettability of the solid substrate, and consequently influencing the freezing behavior. Therefore, it is desirable to establish wetting boundary condition to describe the interaction between the fluid and solid substrate. Based on the geometric relationship, the wetting boundary condition can be formulated as [46]

$$\mathbf{n}_w \cdot \nabla\phi = -\tan\left(\frac{\pi}{2} - \theta\right)|\mathbf{n}_\tau \cdot \nabla\phi|, \tag{39}$$

where $\mathbf{n}_w$ represents the unit normal vector points from the solid wall into the fluids, $\mathbf{n}_\tau$ is the unit vector tangential to solid surface. $\mathbf{n}_w \cdot \nabla\phi$ and $\mathbf{n}_\tau \cdot \nabla\phi$ are the normal and tangential components of $\nabla\phi$, and they can be determined by the second-order schemes [47],

$$n_{\mathrm{w}} \cdot \nabla\phi = \frac{\phi_{x,1} - \phi_{x,0}}{\Delta x}, \tag{40a}$$

$$n_\tau \cdot \nabla\phi = \frac{\partial\phi_{x,1/2}}{\partial x} = 1.5\frac{\partial\phi_{x,1}}{\partial x} - 0.5\frac{\partial\phi_{x,2}}{\partial x}, \tag{40b}$$

where the lattice nodes near the solid substrate are divided into the fluid layer, solid boundary ($y = 1/2$), and ghost layer ($y = 0$). The derivatives of the order parameters can be calculated by a second-order central difference scheme [47],

$$\frac{\partial\phi_{x,y}}{\partial x} = \frac{\partial\phi_{x+1,y} - \partial\phi_{x-1,y}}{2\partial x}. \tag{41}$$

Once the values of the order parameters at the ghost layer are obtained, the gradient of the order parameter and the Laplacian at all fluid nodes can be calculated from Eqs. (38a) and (38b). In addition, the contact angle formulation (39) can be used to simulate the contact line dynamics on smooth surfaces or nonideal surfaces during freezing process.

E. Dimensionless numbers

According to the similarity theory, the numerical solution should be similar to the experimental results as long as they have geometric similarity and the same dimensionless parameters. For the multiphase solidification system considered in this work, it is mainly governed by the following nondimensional parameters:

$$\mathrm{Ste} = \frac{C_p(T_m - T_w)}{L}, \quad \mathrm{Pr} = \frac{\mu_l C_p}{\lambda_l}, \quad \mathrm{Fo} = \frac{\lambda_l t}{\rho_l C_p R_0^2}, \tag{42}$$

where Ste, Pr, and Fo are the Stefan number, Prandtl number, and Fourier number, respectively. The Stefan number characterizes the ratio of sensible heat to latent heat. The Prandtl number represents the ratio of viscosity to thermal diffusivity. The Fourier number represents the ratio of thermal diffusion rate to the rate of heat transfer and can be considered as an dimensionless time.

IV. NUMERICAL RESULTS AND DISCUSSION

In this section, we will test the capability and reliability of the proposed LB method with several typical benchmark problems, including the problem of conduction-induced freezing in a semi-infinite space, the three-phase Stefan problem, freezing droplets on a cold surface, and rising bubbles with solidification, and conduct some comparisons between the present results with the available numerical, analytical, and experimental data reported in some previous works.

A. Conduction-induced freezing problem

We first consider the conduction-induced freezing process of a pure substance in a semi-infinite space to test the present LB method. To simulate this conduction-induced freezing problem, the velocity field is set to be zero, and initially, the computational domain is filled with the liquid-phase substance at a temperature T_0 ($T_0 > T_{\mathrm{m}}$) higher than the melting temperature T_{m}. Then a constant temperature T_b ($T_b < T_{\mathrm{m}}$) is imposed to the left wall ($x = 0$), and the temperature of the right wall is maintained at T_0. Under these conditions, one can obtain the analytical solution of the temperature [40],

$$T(x,t) = \begin{cases} T_b - (T_b - T_{\mathrm{m}})\frac{\mathrm{erf}\left(x/2\sqrt{\alpha_s t}\right)}{\mathrm{erf}\,k} & 0 < x < X_i(t), \quad t > 0 \\ T_0 + (T_{\mathrm{m}} - T_0)\frac{\mathrm{erfc}\left(x/2\sqrt{\alpha_l t}\right)}{\mathrm{erfc}\left(k\sqrt{\alpha_l/\alpha_s}\right)} & x > X_i(t), \quad t > 0 \end{cases}, \tag{43}$$

and the solid-liquid interface in time t,

$$X_i(t) = 2k\sqrt{\alpha_s t}, \tag{44}$$

where k is a constant and can be obtained implicitly from the transcendental equation

$$\frac{C_{p,s}(T_m - T_{\mathrm{b}})}{L\exp(k^2)\,\mathrm{erf}(k)} - \frac{C_{p,l}(T_0 - T_m)\sqrt{\alpha_l/\alpha_s}}{L\exp(k^2\alpha_s/\alpha_l)\,\mathrm{erfc}(k\sqrt{\alpha_s/\alpha_l})} = k\sqrt{\pi}. \tag{45}$$

In simulations, Dirichlet and the periodic boundary conditions are applied in the x and y directions. The thermophysical properties of the pure substance are given by $C_{p,s} = C_{p,l} = 1.0$, $\alpha_s = \alpha_l = 0.4$, $L = 250$, $T_b = -1.0$, $T_0 = 1.0$, and $T_{\mathrm{m}} = 0.0$. Figure 2(b) shows a comparison of the temperature distributions between the present LB results and the analytical solutions at different times, and both of them are in good agreement with each other.

B. Three-phase Stefan problem

In order to accurately predict the droplet freezing process, the volume change during the freezing process should be considered, and thus a source term is added in the continuum equation, as described previously. We now focus on the freezing of pure matter in the semi-infinite space to verify the accuracy of the method in treating volume change. The

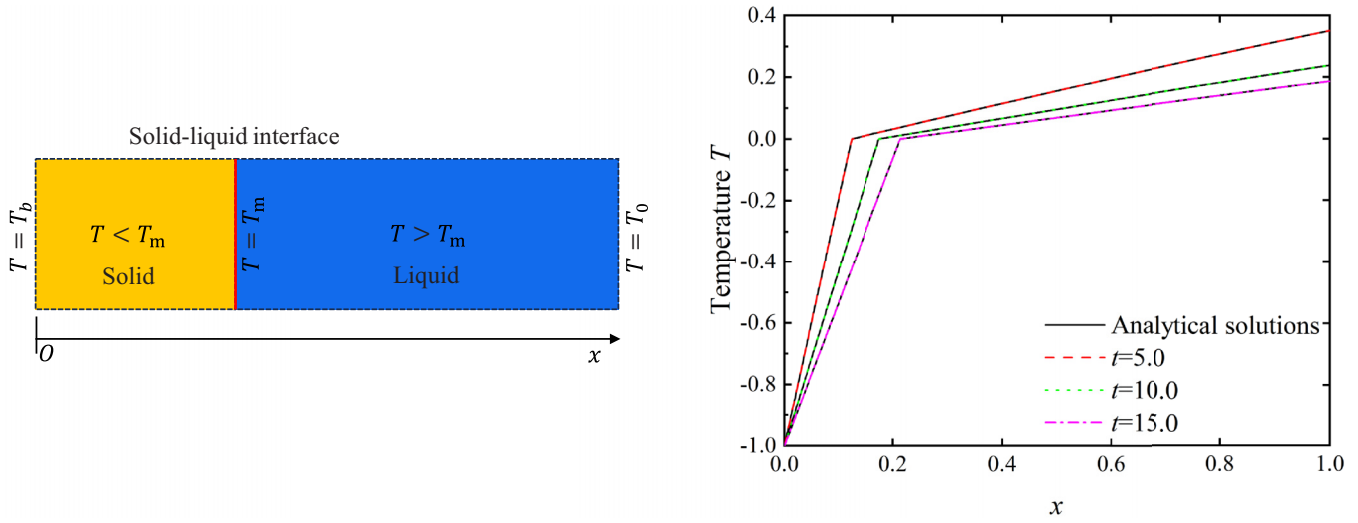

FIG. 2. (a) Schematic diagram of the conduction freezing problem; (b) A comparison of the temperature distributions between LB results and analytical solutions at different times t.

schematic of the problem is depicted in Fig. 3. Initially, the liquid phase and gas phase are uniformly distributed in the regions $0 \leqslant y \leqslant H_0$ and $H_0 \leqslant y \leqslant L$ with the uniform temperature T_0 ($T_0 > T_m$, T_m is the freezing temperature), then a constant temperature $T_w (T_w < T_m)$ is imposed on the bottom wall. To match this setup, the initial profile of the order parameter is given by

$$\phi(x, y) = 0.5 + 0.5 \tanh \frac{2(H_0 - y)}{W}, \tag{46}$$

where the interface width W is set as 5. With the evolution of freezing front from the bottom surface to the free surface, the interfaces among the liquid, gas, and solid phases should be treated simultaneously. Once the freezing of the liquid phase is completed, one can obtain the maximum height of the solid phase, which is denoted by H_f. Based on the mass conservation, the final height of the frozen liquid can be determined from the following equation [22]:

$$H_f = \frac{\rho_l}{\rho_s} H_0. \tag{47}$$

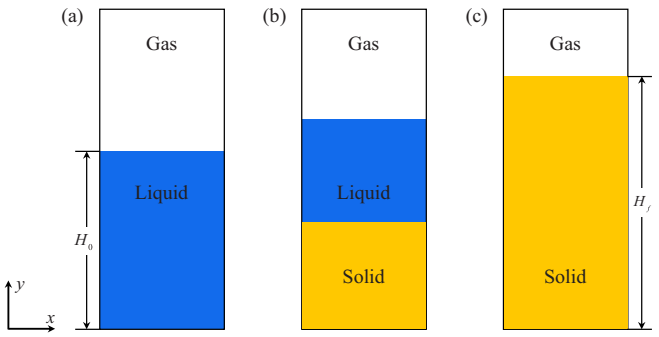

FIG. 3. Schematic of the three-phase Stefan problem. The initial stage before freezing (a), the intermediate stage of partial liquid phase freezing to solid phase (b), the final moment of complete freezing (c).

In our simulations, the grid resolution of the computational region is set to be $N_x \times N_y = 400 \times 10$, the physical parameters are given as $T_0 = 0.1$, $T_w = -2$, $T_m = 0$, Ste = 0.1–0.2, $C_{p,s}/C_{p,l} = 1$, $T_s = T_l = T_m$, and $\lambda_s/\lambda_l = 1$. For the phase, temperature and flow fields, the bottom and top surfaces are the solid walls imposed by the no-flux, Dirichlet, and no-slip boundary condition, while the periodic boundary condition is applied in the horizontal direction. To treat the no-flux and no-slip boundary conditions, the half-way bounce-back scheme is used, while for the Dirichlet boundary condition, the general bounce-back scheme [48] is adopted. Figure 4 shows a comparison of H_f/H_0 between the numerical results and theoretical solution (47), and a good agreement between them can be observed. This indicates that the present LB method can accurately capture the volume change during the freezing process and preserve the mass conservation.

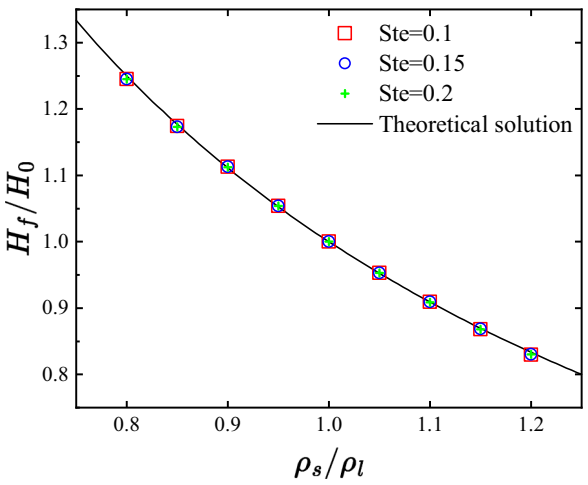

FIG. 4. Comparisons of final dimensionless solid-phase height H_f/H_0 between numerical results and theoretical solution (47) at different values of ρ_s/ρ_l after complete solidification.

TABLE I. Physical properties of water and ice at 0 °C.

Material	Density ρ (kg m^{-3})	Heat capacity C_p (kJ kg^{-1} K^{-1})	Thermal conductivity λ (W m^{-1} K^{-1})	Latent heat L (kJ kg^{-1})
Water	999.8	4.22	0.56	333.4
Ice	917.0	2.02	2.26	–

C. Droplet freezing on a cold surfaces

Droplet freezing on a cold surface is a fundamental heat transfer problem that has been widely used to assess the proposed numerical methods for simulating freezing process. In this part, to show the capacity of the present LB method, we first simulate the droplet freezing on a cold substrate, and then we explore the effects of solid-liquid density ratio and wettability on the droplet freezing.

1. A comparison between the numerical and experimental results

We first conduct a comparison of numerical results with the experimental data reported in Ref. [49]. In the experiment conducted by Hou *et al.* [49], a droplet with a volume of 15 μl is gently deposited on a super-cooled surface at the temperature $T = -29.5\,^{\circ}$C with the contact angle $\theta = 86.4^{\circ}$. Our simulations are carried out in a two-dimensional domain with the grid resolution $N_x \times N_y = 400 \times 200$, and the temperature is set to T_0. Initially, a semicircular droplet with the radius of $R = 40$ is located at the center of the cold substrate. A lower temperature T_w is imposed on the bottom surface after the contact angle of the droplet being equal to the prescribed value θ. In numerical simulations, the distribution of the order parameter is initialized by

$$\phi(x, y) = 0.5 + 0.5 \tanh \frac{2[R - (x - x_0)^2 - (y - y_0)^2]}{W}, \tag{48}$$

where $(x_0, y_0) = (0, N_x/2)$ is the coordinates of droplet center, $W = 5$ is the interface thickness. The periodic boundary condition is applied in the horizontal direction, while the no-slip boundary condition is adopted at the bottom and top boundaries. Based on experimental conditions and the physical properties of water listed in Table I, the following nondimensional parameters, $\mathrm{Pr} = 7.25$, $\mathrm{Ste} = 0.02$, $\lambda_s/\lambda_l = 3.8$, $C_{p,s}/C_{p,l} = 0.5$, $\rho_s/\rho_l = 0.9$, and the contact angle $\theta = 86.4^{\circ}$ are used.

Depending on the temperature fluctuation of water droplet, the freezing process of the droplet on a cold plate can be divided into five stages: liquid stage, nucleation, recalescence stage, solidification stage, and postsolidification stage [8]. Due to the much shorter duration of the nucleation and recalescence stages, compared to the entire freezing period, it is difficult to simulate such a small timescale. Thus, we focus only on the freezing stage based on heat balance, and take the time before nucleation as the initial state [25]. Figure 5 presents a comparison of the freezing process of water droplet on the cold surface between the present results, previous experimental and numerical solutions [49]. In the experiments, the freezing front starts to move from the bottom to the top of the droplet, and the droplet volume expands continuously due to the density difference between water and ice. In this case, the droplet shape expands mainly in the vertical direction instead of the radial direction. It is clear that the present results agree well with the experimental data, and the evolution of the melting front and the change of droplet shape can be captured accurately, which indicates that the present LB method can provide accurate numerical results in the study of the droplet freezing process. However, the numerical results without considering volume change during freezing process are inconsistent with the experimental results [49].

To conduct a quantitative comparison between the present results and some available data, the time evolution of the square of the dimensionless center freezing height H_c is shown in the Fig. 6, in which the results in Ref. [49] are also incorporated. As seen from this figure, the evolution of the freezing front inside the droplet predicted by the LB method has a good

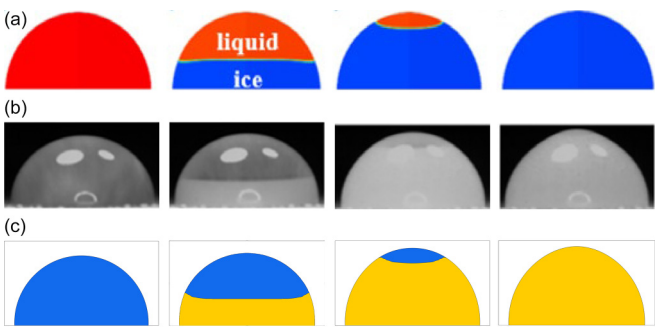

FIG. 5. Comparison of the freezing shapes of droplet at different times: Ref. [49] (a), experiment (b), and present LB back (c), where the gas, liquid, and solid phases are labeled by the white, blue, and orange.

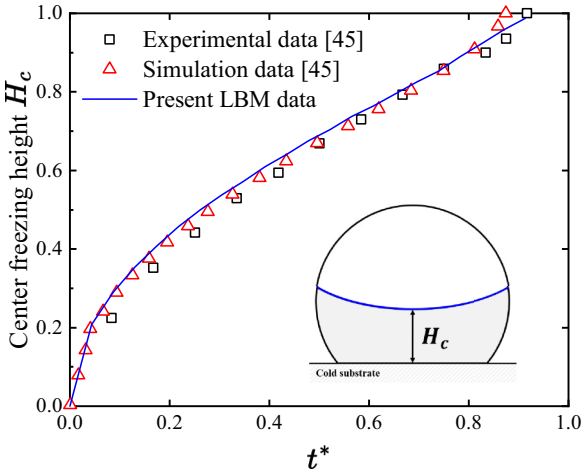

FIG. 6. Comparison of the dimensionless center freezing front height H_c among different works.

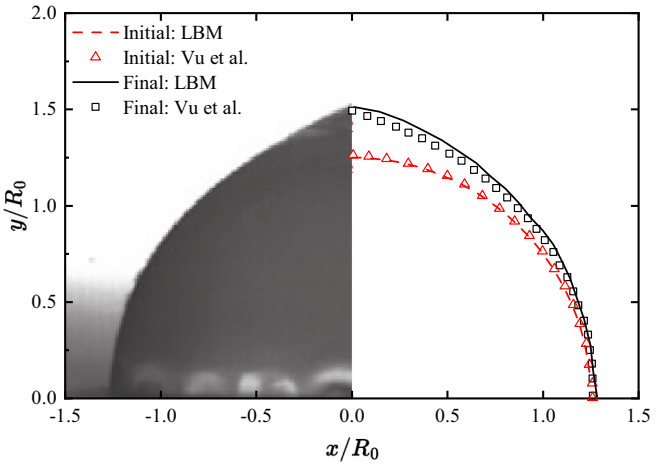

FIG. 7. Comparison of the freezing profile among the present results, numerical results [50], and experimental results [15].

agreement with the previous results [49], which also illustrates that the phase-field-based LB method can be used to predict the freezing process of the water droplet on the cold surface.

In contrast to the spherical cap shape of frozen droplet observed in the experiment [49], the pointed frozen droplet on the cold substrate have also been widely reported. To further validate the ability of present LB method in capturing the tip formation during the freezing process, we perform a comparison of current numerical results with the experimental results of Marin *et al.* [15] and the numerical solution of Vu *et al.* [50]. In the experiments of Marin *et al.* [15], a 4–8 μl droplet with the contact angle $\theta = 90^\circ$ is gently deposited on a cold plate with the constant temperature $T = -44.1\,^\circ$C. Figure 7 shows the initial and final freezing profiles of a droplet, and it can be seen that the present results are in good agreement with the available experimental [15] and numerical data [50]. In addition, the predicted values of aspect ratio H/R by the phase-field base LB method and experiments are 1.18 and 1.16, respectively, H is defined as the final height of the ice drop and R is the radius of the wetted surface area.

2. Freezing characteristics of droplet at different solid-to-liquid density ratios and wettability

The density difference between liquid and solid phases leads to the volume change of droplet during the freezing process. For example, the total volume of the water droplet increases during freezing due to the decrease in average density. In the following, we intend to study the problem of droplet freezing on the cold surface at different solid-to-liquid density ratios. Figure 8 shows the final frozen droplet profiles under different values of the solid-to-liquid density ratio $\gamma = \rho_s/\rho_l$. It can be found from this figure that compared to the initial liquid drop, the volume of droplet expands for $\gamma < 1$, shrinks for $\gamma > 1$, and remains unchanged for $\gamma = 1$. In addition, the expansion and shrinkage of the water droplet mainly occur in the y direction, and only a little expansion and shrinkage in the radial direction are observed during the freezing processes, which is consistent with previous experimental results [51].

To study the effect of surface wettability on the freezing process, we conducted some simulations of droplet freezing on a cold surface with different contact angle varying from $\theta = 30^\circ$ to $\theta = 160^\circ$, while the droplet volume and other parameters are fixed. In our simulations, a droplet with the radius R is placed on a surface with contact angle θ, and once the droplet reaches the prescribed contact angle θ, a temperature field is applied. Figure 9 illustrates the effect of contact angle θ on the dimensionless freezing time t^* at different values of the initial droplet radius R and solid-liquid density ratio γ. As shown in this figure, it is obvious that the freezing time increases with the increase of contact angle θ at the same initial liquid volume, and the increase of volume also leads to an increase in freezing time. We note that the similar results have also been reported in some available numerical simulations [52] and experiments [53,54].

Figures 10 and 11 show the final profiles of frozen droplet at different contact angle, and the dashed line represents the initial droplet with prescribed contact angle θ. It can be seen that for $\gamma < 1$, the gas-liquid interface gradually expands outward and eventually forms a conical tip at the top of the

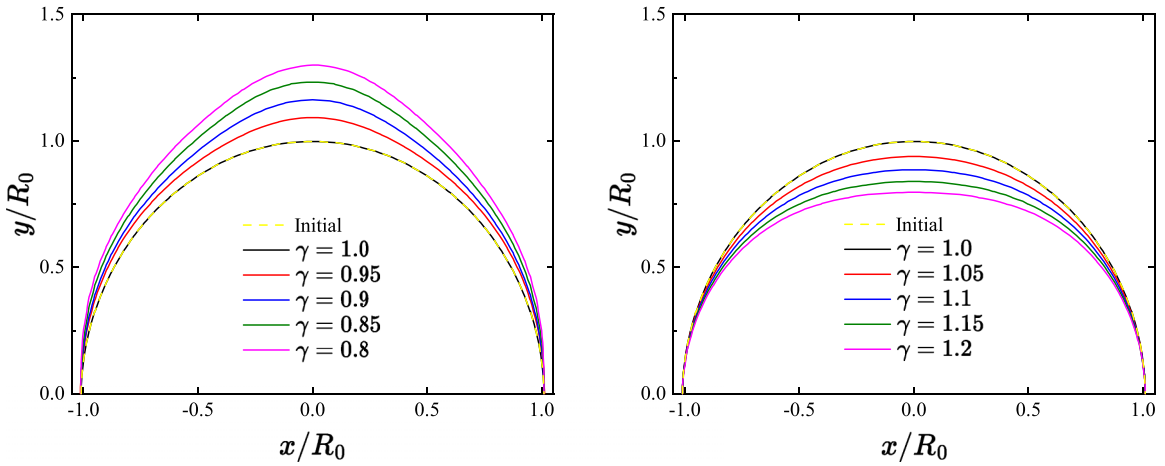

(a) Volume expansion after freezing

(b) Volume shrinkage after freezing

FIG. 8. Effect of solid-to-liquid density ratio $\gamma = \rho_s/\rho_l$ on frozen droplet shape at $\theta = 90^\circ$; the dashed line represents the initial droplet profile.

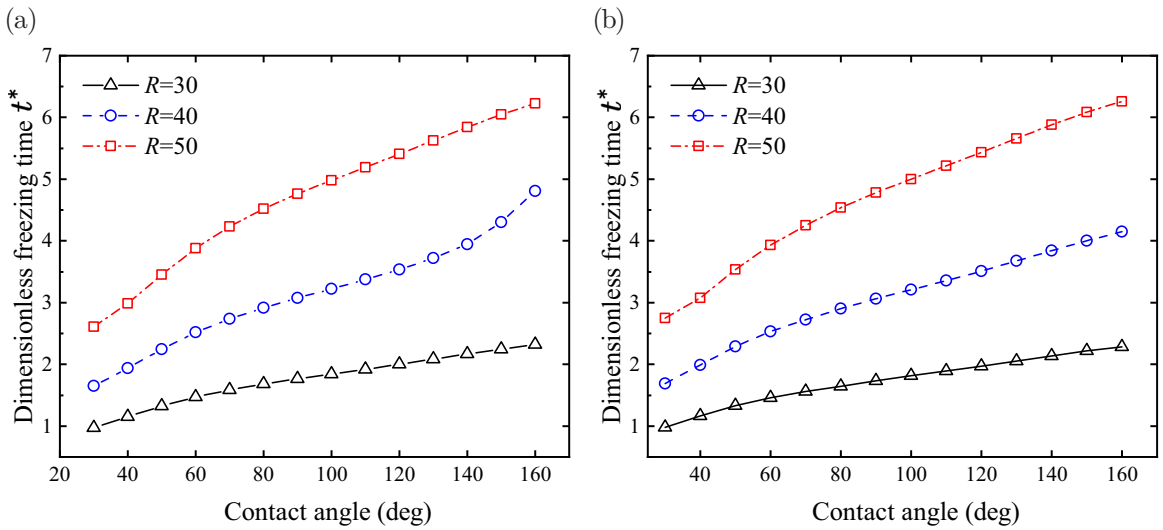

FIG. 9. Effect of contact angle on the dimensionless freezing time t^* of droplet at different values initial radius R: (a) $\gamma = \rho_s/\rho_l < 1$; (b) $\gamma = \rho_s/\rho_l > 1$.

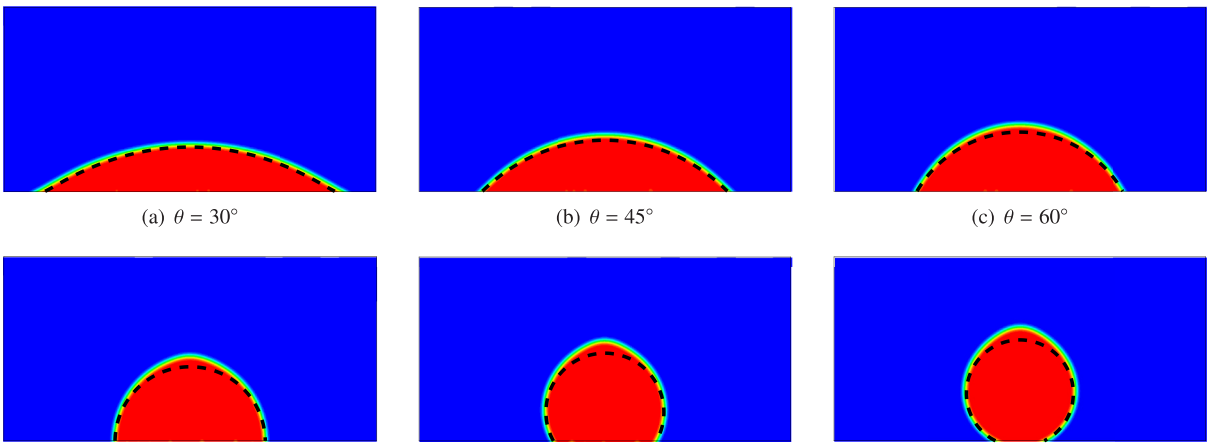

FIG. 10. Final shape of the frozen droplet at different contact angles θ: $R = 40$, Pr $= 7.25$, Ste $= 0.25$, $C_{p,g}/C_{p,l} = 1.0$, and $C_{p,g}/C_{p,s} = 0.5$; the dashed line denotes the initial solidification front.

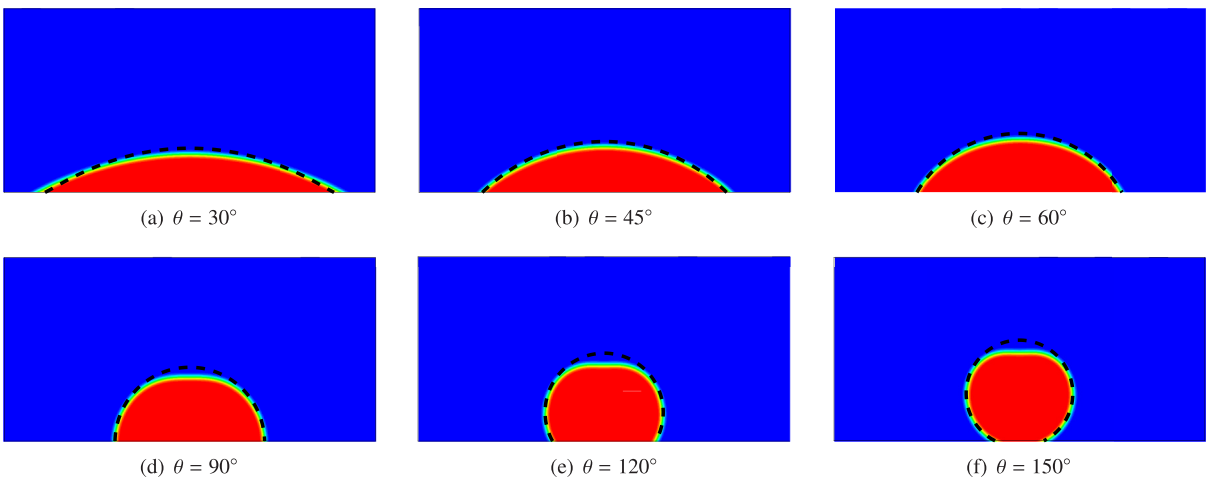

FIG. 11. Final shape of frozen droplet at different contact angles θ: $R = 40$ for $\gamma = 1.1 > 1$, and the dashed line represents the initial solidification front.

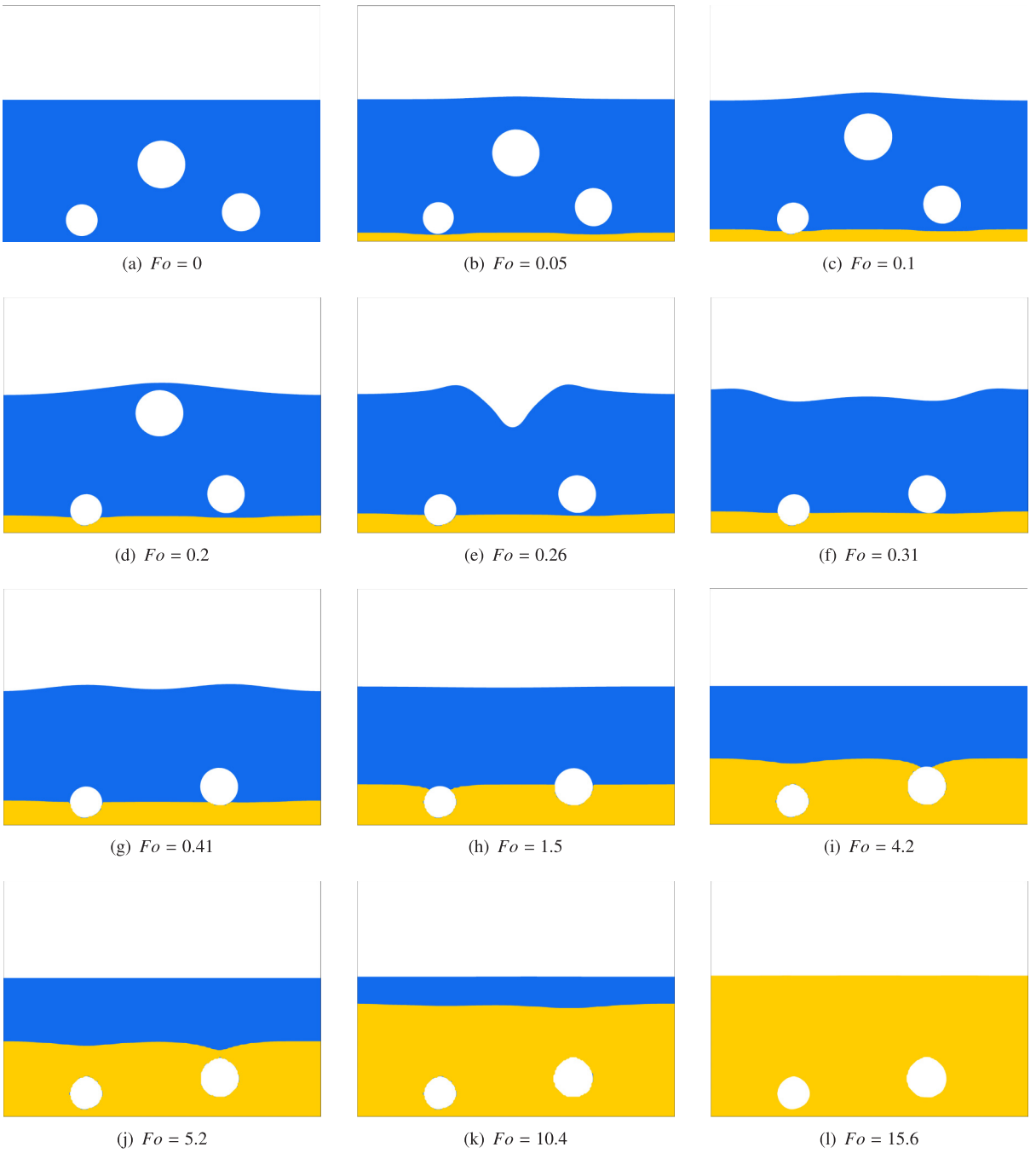

(a) $Fo = 0$ (b) $Fo = 0.05$ (c) $Fo = 0.1$

(d) $Fo = 0.2$ (e) $Fo = 0.26$ (f) $Fo = 0.31$

(g) $Fo = 0.41$ (h) $Fo = 1.5$ (i) $Fo = 4.2$

(j) $Fo = 5.2$ (k) $Fo = 10.4$ (l) $Fo = 15.6$

FIG. 12. Evolution of rising bubbles with solidification, the gas, liquid, and solid phases are filled by the white, blue, and orange.

droplet for a larger contact angle. In contrast, the liquid-gas interface gradually shrinks inward and shrinks in volume for $\gamma > 1$, resulting in the formation of a distinct plateau at the top of the droplet. In addition, a larger contact angle leads to a smaller initial base radius and a larger initial height of the droplet. The former reduces the contact area between the droplet and the cold surface, while the latter increases the thermal resistance. The combined effect of these two factors slows the release of latent heat and the freezing process. Therefore, a larger contact angle results in a lower thermal resistance, which delays the freezing process.

In addition, the rate of freezing in this freezing stage is mainly controlled by the rate of heat transfer from the substrate to the droplet and the rate of dissipation to the surrounding environment via convection. Considering that the droplet is generally very small, the natural convection is practically weak and convective heat transfer can be neglected. In this case, the freezing rate is then mainly controlled by the rate of heat transfer between the droplet and the solid surface, which is described by the following equation [55]:

$$dQ/dt = -h_c L(T_w - T_0), \tag{49}$$

where dQ/dt is the heat transfer rate (J/s), h_c is the heat transfer constant ($\mathrm{J/m^2\,s\,K}$), and L is the contact length (m). According to Eq. (49), the heat transfer by means of conduction is proportional to the contact area or length. For the

same volume of droplet, the contact area of surface with a small contact angle is larger than that with a large contact angle. Therefore, the thermal conductivity decreases with the increase of contact angle, leading to a larger freezing time. We note that these results agree well with previous experimental and analytical results [19,52,54], which demonstrates that the present LB method can accurately predict the freezing process on the cold surfaces.

D. Rising bubbles with solidification

The evolution of gas bubbles during the solidification process has been widely encountered in many engineering applications, such as metalworking and pharmaceutical manufacturing [56,57]. Simulation of the solid-liquid-gas interaction during the solidification process is a challenge due to the complex interfacial dynamics, bubble deformation, and heat transfer across the solid-liquid interface. Recently, Huang *et al.* [58] used a consistent and conservative phase-field model to study the solidification behavior of a liquid column with three gas bubbles, and the numerical results show that the two bubbles at the lower region are eventually captured and frozen as two hollows, while the bubble at the upper region rises upwards under the action of buoyancy force until it breaks and merges with the gas-liquid interface. In this part, to further demonstrate the applicability of present LB method for the solidification process with gas bubbles, we will simulate the freezing process of the liquid column containing bubbles.

The simulations are conducted with a uniform computational mesh $Lx \times Ly = 4l \times 3l$. A liquid column with a height of $H = 1.8l$ is initially located at the bottom wall, and the other region is occupied by gas [seen in Fig. 12(a)]. To be smooth across the interface, the initial order distribution is given by Eq. (46), the liquid column contains three circular gas bubbles with the radii of $0.2l$, $0.24l$, and $0.3l$ from left to right, and their centers are located at $(l, 0.3l)$, $(2l, 1l)$, and $(3l, 0.4l)$. The initial temperature of the system is set to T_0, and a lower temperature T_w is adopted on the bottom wall. The periodic boundary condition is applied in the horizontal direction, the bottom and top boundaries are two solid walls, and the bounce back and anti-bounce-back schemes are used to treat the nonslip and Dirichlet boundary conditions of flow and temperature fields. In addition, all the physical parameters used in our simulations are $\mathrm{Pr} = 7.25$, $\mathrm{Ste} = 0.02$, $\lambda_s/\lambda_l = 3.8$, $C_{p,s}/C_{p,l} = 0.5$, and $\rho_s/\rho_l = 0.9$. Furthermore, the surface tension force in Eq. (5) is modified by $\mathbf{F}_s = f_s \mu_\phi \nabla\phi$, which ensures that the surface tension force acts only at the interface between the gas and liquid phases. Under the assumption of the Boussinesq approximation, the buoyancy force can be given as $\mathbf{F}_g = -\rho_0 \mathbf{g}\beta(T - T_{\mathrm{ref}})$, where $\mathbf{g}$, β, and T_{ref} are the acceleration of gravity, volumetric expansion coefficient and reference temperature, respectively.

Figure 12 plots the solidification process of liquid pool with gas bubbles, in which the solid, liquid, and gas phases are filled with the white, blue, and orange. In the initial stage, the solidified phase begins to develop near the cold substrate, and the freezing front gradually moves upward. As the solidified phase grows, two bubbles located in the lower region gradually form two hollows. Due to the lower thermal conductivity of the gas phase than that of the liquid phase, the solidification is slower right above the two trapped gas bubbles, resulting in a V-shaped solid-liquid interface, as shown in Fig. 12(l). At the same time, the gas bubbles at the upper region gradually rise to the liquid-gas interface under the action of buoyancy and eventually rupture. Finally, the liquid pool completely solidifies, with two hollows formed by two gas bubbles located in the lower region. We would like to point out that the present results are in agreement with those reported in Ref. [58], which indicates that the present LB method can accurately capture the evolution of gas bubbles during the solidification process. In addition, the Mach number ($\mathrm{Ma} = u/c_s$) is less than 0.1 in our simulations, which can be used to reduce compressibility error and nonphysical oscillation.

V. CONCLUSIONS

In this work we propose a phase-field LB method to simulate the freezing process in a gas-liquid-solid system where the volume expansion or shrinkage caused by the density difference between liquid and solid is considered through adding a source term to the continuity equation. The model is first validated by simulating the solidification of a liquid column, and the results show that the proposed LB method is accurate in the study of the liquid-solid phase change with the volume change. Then the LB method is applied to investigate the freezing dynamics of droplet on a cold substrate, and it is found that the present numerical results are in good agreement with the experimental data. Furthermore, we focus on the effects of several key parameters on the freezing of sessile droplet on a cold surface, such as the solid-to-liquid density ratio, the contact angle, and volume of droplet, and find that the solidification time increases with the increase of contact angle and droplet volume, which is consistent with previous experimental results. In addition, the solid-to-liquid density ratio has a significant influence on the evolution of the droplet shape. For the case with volume expansion ($\rho_s < \rho_l$), the frozen droplet tends to form a conical shape on the upper surface, while for the case with volume shrinkage ($\rho_s > \rho_l$), a distinctive plateau is formed at the top of the frozen droplet. Finally, a more challenging problem of liquid column solidification with bubbles is also considered, and the rising and deformation behavior of bubbles during solidification can be captured by the present LB method. The numerical results show that the present LB method is effective and accurate in the study of the freezing/solidification problems.

ACKNOWLEDGMENTS

This work was financially supported by the National Natural Science Foundation of China (Grants No. 12072127 and No. 123B2018), the Interdisciplinary Research Program of Hust (Grants No. 2023JCJY002 and No. 2024JCYJ001), and the Fundamental Research Funds for the Central Universities, Hust (Grants No. 2023JY-CXJJ046 and No. YCJJ20241101). The computation was completed on the HPC Platform of Huazhong University of Science and Technology.

[1] L. S. Yao and J. Prusa, Melting and freezing, Adv. Heat Transfer **19**, 1 (1989).

[2] B. C. Bernstein, Regional and local influences on freezing drizzle, freezing rain, and ice pellet events, Weather Forecast. **15**, 485 (2000).

[3] M. Liu, W. Saman, and F. Bruno, Development of a novel refrigeration system for refrigerated trucks incorporating phase change material, Appl. Energy **92**, 336 (2012).

[4] Y. Cao, W. Tan, and Z. Wu, Aircraft icing: An ongoing threat to aviation safety, Aerosp. Sci. Technol. **75**, 353 (2018).

[5] H. L. Wei, J. Mazumder, and T. DebRoy, Evolution of solidification texture during additive manufacturing, Sci. Rep. **5**, 16446 (2015).

[6] D. L. Archer, Freezing: An underutilized food safety technology? Int. J. Food Microbiol. **90**, 127 (2004).

[7] Y. Cao and M. Xin, Numerical simulation of supercooled large droplet icing phenomenon: A review, Arch. Comput. Methods Eng. **27**, 1231 (2020).

[8] A. Tiwari, R. Samanta, and H. Chattopadhyay, Droplet solidification: Physics and modelling, Appl. Therm. Eng. **228**, 120515 (2023).

[9] D. M. Anderson, M. G. Worster, and S. H. Davis, The case for a dynamic contact angle in containerless solidification, J. Cryst. Growth **163**, 329 (1996).

[10] W. W. Schultz, M. G. Worster, and D. M. Anderson, Solidifying sessile water droplets, in *Interactive Dynamics of Convection and Solidification*, edited by P. Ehrhard, D. S. Riley, and P. H. Steen (Springer, Dordrecht, 2001), pp. 209–226.

[11] V. S. Ajaev and S. H. Davis, Boundary-integral simulations of containerless solidification, J. Comput. Phys. **187**, 492 (2003).

[12] H. Hu and Z. Jin, An icing physics study by using lifetime-based molecular tagging thermometry technique, Int. J. Multiphase Flow **36**, 672 (2010).

[13] G. Chaudhary and R. Li, Freezing of water droplets on solid surfaces: An experimental and numerical study, Exp. Therm Fluid Sci. **57**, 86 (2014).

[14] O. R. Enríquez, Á. G. Marín, K. G. Winkels, and J. H. Snoeijer, Freezing singularities in water drops, Phys. Fluids **24**, 091102 (2012).

[15] A. G. Marín, O. R. Enriquez, P. Brunet, P. Colinet, and J. H. Snoeijer, Universality of tip singularity formation in freezing water drops, Phys. Rev. Lett. **113**, 054301 (2014).

[16] M. Schremb and C. Tropea, Solidification of supercooled water in the vicinity of a solid wall, Phys. Rev. E **94**, 052804 (2016).

[17] H. Zeng, S. Lyu, D. Legendre, and C. Sun, Influence of gravity on the freezing dynamics of drops on a solid surface, Phys. Rev. Fluids **7**, 103605 (2022).

[18] X. Zhang, X. Wu, J. Min, and X. Liu, Modelling of sessile water droplet shape evolution during freezing with consideration of supercooling effect, Appl. Therm. Eng. **125**, 644 (2017).

[19] M. Tembely and A. Dolatabadi, A comprehensive model for predicting droplet freezing features on a cold substrate, J. Fluid Mech. **859**, 566 (2019).

[20] Z. Zhu, X. Zhang, Y. Zhao, X. Huang, and C. Yang, Freezing characteristics of deposited water droplets on hydrophilic and hydrophobic cold surfaces, Int. J. Therm. Sci. **171**, 107241 (2022).

[21] T. V. Vu, G. Tryggvason, S. Homma, and J. C. Wells, Numerical investigations of drop solidification on a cold plate in the presence of volume change, Int. J. Multiphase Flow **76**, 73 (2015).

[22] H. Shetabivash, A. Dolatabadi, and M. Paraschivoiu, A multiple level-set approach for modelling containerless freezing process, J. Comput. Phys. **415**, 109527 (2020).

[23] S. Lyu, K. Wang, Z. Zhang, A. Pedrono, C. Sun, and D. Legendre, A hybrid VOF-IBM method for the simulation of freezing liquid films and freezing drops, J. Comput. Phys. **432**, 110160 (2021).

[24] J. Sun, J. Gong, and G. Li, A lattice Boltzmann model for solidification of water droplet on cold flat plate, Int. J. Refrig. **59**, 53 (2015).

[25] C. Zhang, H. Zhang, W. Fang, Y. Zhao, and C. Yang, Axisymmetric lattice Boltzmann model for simulating the freezing process of a sessile water droplet with volume change, Phys. Rev. E **101**, 023314 (2020).

[26] W. Xiong and P. Cheng, Mesoscale simulation of a molten droplet impacting and solidifying on a cold rough substrate, Int. Commun. Heat Mass Transfer **98**, 248 (2018).

[27] W. Xiong and P. Cheng, Numerical investigation of air entrapment in a molten droplet impacting and solidifying on a cold smooth substrate by 3D lattice Boltzmann method, Int. J. Heat Mass Transf. **124**, 1262 (2018).

[28] Y. Zhang, B. Dong, P. Wang, F. Geng, L. Zhang, Y. Qin, C. Chen, and W. Li, Investigation of ice evolution during methane hydrate dissociation at different initial temperatures in microporous media, Energy **266**, 126484 (2023).

[29] O. R. Mohammadipour and X. Duan, A new lattice Boltzmann model for liquid–solid phase transition and its application in the simulation of sessile droplet solidification—Focusing on volume change, J. Fluid Mech. **978**, A10 (2024).

[30] L. Chen, Q. Kang, Y. Mu, Y.-L. He, and W.-Q. Tao, A critical review of the pseudopotential multiphase lattice Boltzmann model: Methods and applications, Int. J. Heat Mass Transf. **76**, 210 (2014).

[31] H. Wang, X. Yuan, H. Liang, Z. Chai, and B. Shi, A brief review of the phase-field-based lattice Boltzmann method for multiphase flows, Capillarity **2**, 33 (2019).

[32] H. Liang, J. Xu, J. Chen, J. Chen, H. Wang, Z. Chai, and B. Shi, Phase-field-based lattice Boltzmann modeling of large-density-ratio two-phase flows, Phys. Rev. E **97**, 033309 (2018).

[33] D. Jacqmin, Calculation of two-phase Navier–Stokes flows using phase-field modeling, J. Comput. Phys. **155**, 96 (1999).

[34] M. Raessi and J. Mostaghimi, Three-dimensional modeling of density variation due to phase change in complex free surface flows, Numer. Heat Transf. B **47**, 507 (2005).

[35] D. R. Noble and J. R. Torczynski, A lattice-Boltzmann method for partially saturated computational cells, Int. J. Mod. Phys. C **09**, 1189 (1998).

[36] Y. Zhao, L. Wang, Z. Chai, and B. Shi, Comparative study of natural convection melting inside a cubic cavity using an improved two-relaxation-time lattice Boltzmann model, Int. J. Heat Mass Transf. **143**, 118449 (2019).

[37] K. He, Y. Zhao, and L. Wang, Numerical investigation on electrohydrodynamic enhancement of solid–liquid phase change in three-dimensional cavities, Int. J. Multiphase Flow **168**, 104562 (2023).

[38] J. Liu, C. Huang, Z. Chai, and B. Shi, A diffuse-interface lattice Boltzmann method for fluid–particle interaction problems, Comput. Fluids **233**, 105240 (2022).

[39] S. Chakraborty and D. Chatterjee, An enthalpy-based hybrid lattice-Boltzmann method for modelling solid–liquid phase transition in the presence of convective transport, J. Fluid Mech. **592**, 155 (2007).

[40] R. Huang, H. Wu, and P. Cheng, A new lattice Boltzmann model for solid–liquid phase change, Int. J. Heat Mass Transf. **59**, 295 (2013).

[41] W. Shyy, *Computational Fluid Dynamics with Moving Boundaries* (CRC Press, Boca Raton, FL, 1995).

[42] X. Yuan, Z. Chai, H. Wang, and B. Shi, A generalized lattice Boltzmann model for fluid flow system and its application in two-phase flows, Comput. Math. Appl. **79**, 1759 (2020).

[43] C. Zhan, Z. Chai, B. Shi, P. Jiang, S. Geng, and D. Sun, A diffuse-interface lattice Boltzmann method for the dendritic growth with thermosolutal convection, Commun. Comput. Phys. **33**, 1164 (2023).

[44] C. Zhan, Z. Chai, and B. Shi, A ternary phase-field model for two-phase flows in complex geometries, Physica D **460**, 134087 (2024).

[45] X. Liu, Z. Chai, and B. Shi, Improved hybrid Allen-Cahn phase-field-based lattice Boltzmann method for incompressible two-phase flows, Phys. Rev. E **107**, 035308 (2023).

[46] H. Ding and P. D. M. Spelt, Wetting condition in diffuse interface simulations of contact line motion, Phys. Rev. E **75**, 046708 (2007).

[47] H. Liang, H. Liu, Z. Chai, and B. Shi, Lattice Boltzmann method for contact-line motion of fluids with high density ratio, Phys. Rev. E **99**, 063306 (2019).

[48] T. Zhang, B. Shi, Z. Guo, Z. Chai, and J. Lu, General bounce-back scheme for concentration boundary condition in the lattice-Boltzmann method, Phys. Rev. E **85**, 016701 (2012).

[49] J. Hou, J. Gong, X. Wu, and Q. Huang, Numerical study on impacting-freezing process of the droplet on a lateral moving cold superhydrophobic surface, Int. J. Heat Mass Transf. **183**, 122044 (2022).

[50] T. V. Vu, Axisymmetric forced convection solidification of a liquid drop on a cold plate, Int. J. Multiphase Flow **107**, 104 (2018).

[51] M. Song, C. Dang, T. Higashi, and E. Hihara, Review of experimental data associated with the solidification characteristics of water droplets on a cold plate surface at the early frosting stage, Energy Buildings **223**, 110103 (2020).

[52] X. Zhang, X. Liu, X. Wu, and J. Min, Simulation and experiment on supercooled sessile water droplet freezing with special attention to supercooling and volume expansion effects, Int. J. Heat Mass Transf. **127**, 975 (2018).

[53] H. F. Zhang, Y. Zhao, R. Lv, and C. Yang, Freezing of sessile water droplet for various contact angles, Int. J. Therm. Sci. **101**, 59 (2016).

[54] L. Huang, Z. Liu, Y. Liu, Y. Gou, and L. Wang, Effect of contact angle on water droplet freezing process on a cold flat surface, Exp. Therm Fluid Sci. **40**, 74 (2012).

[55] L. Oberli, D. Caruso, C. Hall, M. Fabretto, P. J. Murphy, and D. Evans, Condensation and freezing of droplets on superhydrophobic surfaces, Adv. Colloid Interface Sci. **210**, 47 (2014).

[56] D. Sun, M. Zhu, J. Wang, and B. Sun, Lattice Boltzmann modeling of bubble formation and dendritic growth in solidification of binary alloys, Int. J. Heat Mass Transf. **94**, 474 (2016).

[57] P. D. Lee, A. Chirazi, and D. See, Modeling microporosity in aluminum–silicon alloys: A review, J. Light Met. **1**, 15 (2001).

[58] Z. Huang, G. Lin, and A. M. Ardekani, A consistent and conservative phase-field model for thermo-gas-liquid-solid flows including liquid-solid phase change, J. Comput. Phys. **449**, 110795 (2022).